Astron. Astrophys. 359, 759–765 (2000)

ASTRONOMY AND ASTROPHYSICS

The effect of random flow on solar acoustic waves

K. Murawski[1] **and E.N. Pelinovsky**[2]

[1] Department of Environmental Physics, Technical University of Lublin, ul. Nadbystrzycka 40a, 20-618 Lublin, Poland
[2] Institute of Applied Physics, 46 Ul'anova Street 603600, Nizhny Novgorod, Russia

Received 16 February 2000 / Accepted 24 April 2000

Abstract. We examine the influence of a random flow that occurs in the convection zone on frequencies of the solar acoustic oscillations. Using a perturbative method the dispersion relation is derived in the case of a random flow that is parallel to the wave propagation. This relation is subsequently solved numerically for various parameters of the random field to find the frequencies of the random acoustic waves. The numerical results reveal that these waves can be both amplified and damped by the random flow; also their frequencies can be higher and lower than the frequencies of the coherent acoustic waves. The amplification and frequency increase are more pronounced for low spherical harmonic degree l, stronger random flow, and lower spatial correlation length. These analytical findings are tested against numerical simulations for the full set of linear equations, without introducing a weak random field approximation. Numerical results reveal for the first time wave amplification and frequency decrease of the sound waves.

Key words: convection – Sun: atmosphere – Sun: granulation – Sun: oscillations – turbulence

1. Introduction

Recently in solar physics a certain interest has arisen to the problem of interaction of waves and steady flows. In particular, flows can affect MHD waves trapped by magnetic flux tubes, modifying dispersion relations and changing wave cutoffs (Nakariakov & Roberts 1995). Also, it was shown (Joarder et al. 1997) that in the photosphere and below, observationally registered down-flows can cause negative energy wave effects, leading to instability and over-stability of the waves due to their interaction with the flows. In Nakariakov et al. (1998), it was found that even very weak flows, as long as they had sufficiently sharp gradients, can dramatically affect propagation of the waves, causing enhanced coupling of different wave modes. Thus, it is believed that the wave-flow interactions play a very important role in the dynamics of the solar plasma.

The Sun exhibits global oscillations which are influenced by a turbulent flow in the convection zone. The first evidence of these oscillations was provided by Leighton et al. (1962) who measured the Doppler shifts of photospheric spectral lines. Subsequently, it was proposed by Ulrich (1970) that acoustic waves were the cause of the Doppler shifts. As pressure provides the restoring force for these oscillations, they are called *p*-modes. Since the observable properties of solar global oscillations depend on the underlying solar structure and dynamics, they provide a potential tool for probing the solar interior (Gough 1994).

Although recent investigations prove that new solar models closely describe the Sun, there are still significant discrepancies between the predictions and the observations of the *p*-modes. As these discrepancies depend on frequency but are nearly independent of the spherical harmonic degree l it is supposed that the discrepancies are caused by effects that occur close to the solar surface. In this paper we investigate a possible cause of these discrepancies: stochastic flow as it affects *p*-mode frequencies and their line-widths.

The influence of convection on solar oscillations was discussed by several authors. In particular, Brown (1984), while considering vertical velocity perturbations, suggested that such perturbations cause a frequency decrease of sufficient magnitude to produce an observable effect. Lavely & Ritzwoller (1992) used perturbation theory to investigate the effects of steady-state convection on the *p*-mode line-widths and frequencies. They showed that large-scale convective flows have a systematic effect on the line-widths of the *p*-modes of a low spherical harmonic degree $l < 100$. It has been shown by Kosovichev (1995) that the turbulent pressure decreases the sound speed in the external regions of the convection zone, leading to reduction of the *p*-mode frequencies. Gruzinov (1998) applied perturbation theory, but with an emphasis on finding analytical expressions for the frequency shift. Zhugzhda (1998) considered corrections arising from a sinusoidal perturbation to the sound speed and the vertical velocity, ignoring any horizontal flows. He found that the result is a frequency reduction which is proportional to both frequency and spherical harmonic l. Swisdak & Zweibel (1999) implemented an approach for determining the frequencies of the *p*-modes in a convective envelope. This approach is based on the ray approximation and the method of adiabatic switching to seek the eigenfrequencies of a Hamiltonian system. As a result, large-scale convective perturbations can generate downward frequency shifts which are second-order in the perturbation strength. Bömer & Rüdiger (1999) examined

Send offprint requests to: K. Murawski
(kamur@akropolis.pol.lublin.pl)

the influence of turbulence by the Reynolds stress on a reduction of the frequencies of the *p*-modes.

This paper is organized as follows. The next section presents linear equations which describe the interaction between the flow and the acoustic waves. Sect. 3 presents the random dispersion relation which is solved numerically for the case of a space-dependent random flow as well as for a time-dependent flow. Sect. 4 is devoted to numerical simulations of linear hydrodynamic equations. The paper is concluded by a short summary.

2. Linear equations

We consider a gravity-free plasma which is described by ideal hydrodynamic equations. At a uniform equilibrium,

$$\varrho_0 = const, \quad p_0 = const, \tag{1}$$

the plasma can flow with the speed $\boldsymbol{V}_0(x,t)$ which is assumed to be small, viz. $V_0 < c_0$, where c_0 is the sound speed.

The present model strictly applies only to waves propagating in one dimension with parallel random flows. Although this is an important class to consider, it has to be admitted that the solar case is substantially different. In particular, solar *p*-modes propagate in three dimensions and convective flows are characterized by strong up- and down-flows with relatively weak horizontal motions. However, if any inhomogeneity of the solar plasma exhibits large spatial scales in comparison to the wavelength of the *p*-mode, then the *p*-modes can be well approximated by acoustic waves (Swisdak & Zweibel 1999). Using this approximation is justified by the fact that we are more concerned with the physical insight we can derive from this model than its self-consistency.

As the amplitude of the flow ($1\ \mathrm{m\,s^{-1}}$) that is associated with the *p*-modes is small in comparison to the sound speed $\sim 10\,\mathrm{km\,s^{-1}}$ we are allowed to apply the linear theory. Consequently, small perturbations to this equilibrium can be described by the linearized equations:

$$V_t + V_0 V_x + V_{0x} V = -\frac{1}{\varrho_0} p_x, \tag{2}$$

$$p_t + V_0 p_x + \gamma V_{0x} p = -\gamma p_0 V_x, \tag{3}$$

where V is the perturbed flow speed in the x-direction, p is the perturbed pressure, and $\gamma = 5/3$ is the specific heat ratio. The indices x and t denote the space and time derivatives, respectively.

Eqs. (2) and (3) describe the coupling between the flow V and the pressure p; perturbations in p excite oscillations in V and vice versa, a signal in V drives oscillations in p. The terms $V_{0x}V$ and $\gamma V_{0x}p$ correspond to damping (amplification) of perturbations if $V_{0x} > 0$ ($V_{0x} < 0$). The terms $V_0 V_x$ and $V_0 p_x$ are responsible for the Doppler shift of the frequency.

3. Random dispersion relation

Eqs. (2) and (3) describe the sound wave which propagates in a flowing plasma. In a motionless ($V_0 = 0$) plasma the dispersion relation for the acoustic wave reads

$$\omega^2 = c_0^2 k^2, \tag{4}$$

where ω and k are the frequency and the x-component of the wavevector, respectively.

We assume now that the speed $\boldsymbol{V}_0$ is random. As a consequence of that all perturbed quantities have to be expanded as

$$V = \langle V \rangle + V', \quad p = \langle p \rangle + p'. \tag{5}$$

Here, the symbol $\langle\rangle$ denotes the ensemble average and the prime corresponds to the random field which is assumed to be centered, viz.

$$\langle V' \rangle = \langle p' \rangle = 0. \tag{6}$$

Using the perturbative method of Howe (1971) in which a weak random field approximation is applied, we obtain a turbulent dispersion relation

$$\omega^2 - c_0^2 k^2 = \int_{-\infty}^{\infty}\int_{-\infty}^{\infty} \{ c_0^2 \frac{k\hat{k}}{\hat{\omega}^2 - c_0^2\hat{k}^2} [k\hat{k}\hat{R}_0 - i\gamma\hat{k}\hat{R}_1 -$$

$$k\frac{\hat{\omega}}{\omega}(i\hat{R}_1 - ik\hat{R}_0)] - \frac{c_0^2 k}{\hat{\omega}^2 - c_0^2\hat{k}^2}[ik\hat{k}\hat{R}_1 +$$

$$\gamma\hat{k}\hat{R}_2 + k\frac{\hat{\omega}}{\omega}(ik\hat{R}_1 + R_2)] +$$

$$\frac{\omega\hat{\omega}}{\hat{\omega}^2 - c_0^2\hat{k}^2}[k\hat{k}\hat{R}_0 - i\gamma\hat{k}\hat{R}_1 - ik\frac{\hat{\omega}}{\omega}(ik\hat{R}_0 + \hat{R}_1)]$$

$$-\frac{\gamma\omega\hat{\omega}}{\hat{k}(\hat{\omega}^2 - c_0^2\hat{k}^2)}[ik\hat{k}\hat{R}_1 + \gamma\hat{k}\hat{R}_2 + k\frac{\hat{\omega}}{\omega}(ik\hat{R}_1 + \hat{R}_2)] +$$

$$k(i\hat{R}_1 - k\hat{R}_0) + \gamma\frac{k}{\hat{k}}(ik\hat{R}_1 + \hat{R}_2)\}\, d\hat{k}\, d\hat{\omega}. \tag{7}$$

Here, $\hat{R}_i(\omega - \hat{\omega}, k - \hat{k})$, $i = 0, 1, 2$, is the Fourier transform of the correlation functions:

$$R_0(x - X, t - T) = \langle V_0(x,t) V_0(X,T) \rangle, \tag{8}$$

$$R_1(x - X, t - T) = \langle V_{0x}(x,t) V_0(X,T) \rangle, \tag{9}$$

$$R_2(x - X, t - T) = \langle V_{0x}(x,t) V_{0X}(X,T) \rangle. \tag{10}$$

It is noteworthy that the right hand side of Eq. (7) contains a random correction to the acoustic dispersion relation. In the case of stationary plasma ($V_0 = 0$) this equation reduces to Eq. (4) which is valid for a coherent acoustic wave. The random flow modifies wave frequencies as a result of scattering which can be considered as a nonlinear interaction between the incident wave with (k_1, ω_1), the scattering wave with (k_2, ω_2), and the "inhomogeneous wave" with (k_3, ω_3). As in any nonlinear process, the interaction is effective if wavevectors and frequencies satisfy the resonance conditions (e.g., Rabinovich & Trubetskov 1989):

$$k_1 \mp k_2 = \pm k_3, \tag{11}$$

$$\omega_1 \mp \omega_2 = \pm \omega_3. \tag{12}$$

In the case of a space-dependent random field, the frequency of the inhomogeneous wave is zero. Therefore, the scattered

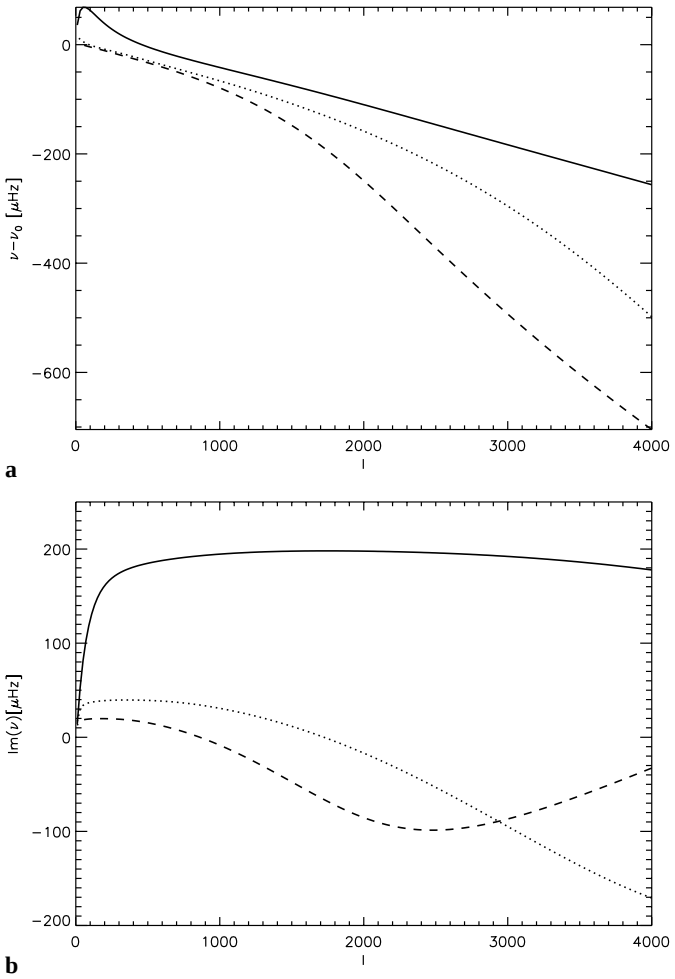

Fig. 1a and b. The frequency difference $\nu - \nu_0$ and the imaginary part of the frequency ν as functions of the spherical harmonic degree l for the case of the space-dependent random flow with variance $\sigma_0 = 1\,\mathrm{km\,s^{-1}}$. The solid, dotted and broken lines represent the data obtained from Eq. (16) for $l_x = 0.2\,\mathrm{Mm}$, $l_x = 1\,\mathrm{Mm}$, and $l_x = 2\,\mathrm{Mm}$, respectively. For high values of l, the effect of the random flow is to reduce frequencies and damp the acoustic waves. For low values of l the acoustic waves can be amplified and their frequencies can be shifted up by the random flow.

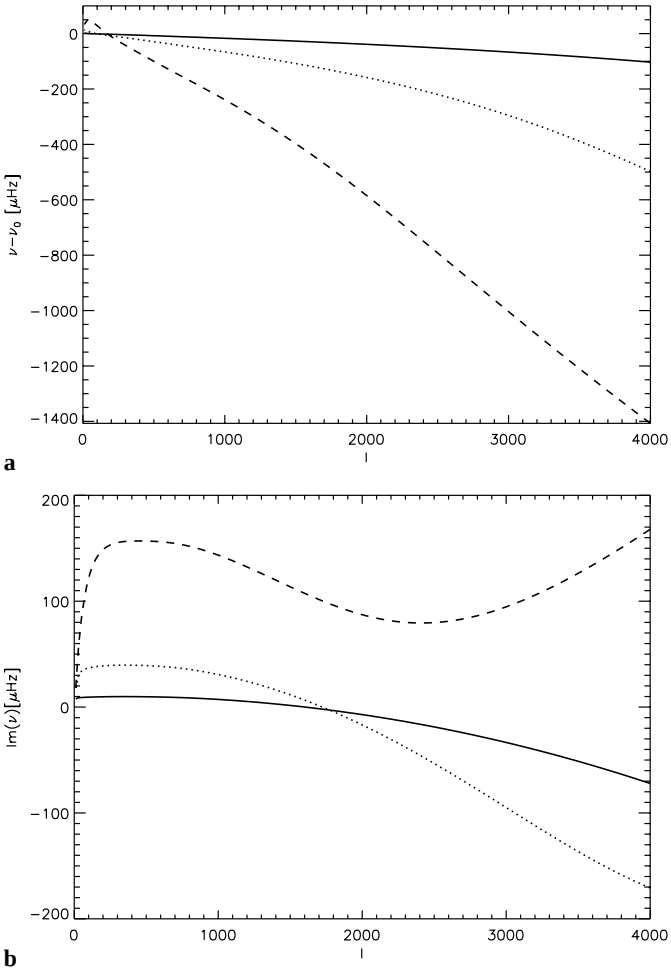

Fig. 2a and b. As in Fig. 1 but for a random flow with correlation length $l_x = 1\,\mathrm{Mm}$ and variance $\sigma_0 = 0.5\,\mathrm{km\,s^{-1}}$ (solid line), $\sigma_0 = 1\,\mathrm{km\,s^{-1}}$ (dotted line), and $\sigma_0 = 2\,\mathrm{km\,s^{-1}}$ (broken line). A stronger random flow reduces the frequencies of the acoustic waves more strongly as well as amplifying them further. The frequency-reduction effect is more pronounced for higher values of l.

wave should have the same frequency as the incident wave. Then, from dispersion relation (4) it follows that $k_2^2 = k_1^2$. As a consequence, from Eq. (11) we have: a) forward scattering with $k_2 = k_1$, $k_3 = 0$; b) backward scattering with $k_2 = -k_1$, $k_3 = 2k_1$. Every set of k_1, k_2, k_3 defines the interacting triad. This is the Bragg condition for wave scattering. This scattering scenario is similar in the case of spatial or temporal random fields. The corresponding wavenumbers and frequencies of the scattered and inhomogeneous waves can be found from Eqs. (11) and (12).

The energetics of the wave interactions in media for which equilibrium conditions are satisfied can be described with a use of the Manley-Rowe relations (e.g., Pelinovsky 1979, Rabinovich & Trubetskov 1989). In this case, if the incident wave interacts with the inhomogeneous wave of low frequency a part of its energy is transformed into energy of the scattered wave. As a consequence of that, the energy of the incident wave is decreased. On the other hand, if the incident wave interacts with the inhomogeneous wave of high frequency its energy and the energy of the scattered wave is increased due to parametric instability of the high-frequency noise. A global picture of the interaction depends on the number of triads for which the incident wave frequency is increased or decreased. This scheme was used by Pelinovsky (1979) for analysis of the wave propagation in a random inhomogeneous ocean. Unfortunately, the case of a non-equilibrium medium, such as one with a random flow, is more complicated. In this case, the Manley-Rowe relations are not satisfied and the above scheme cannot be applied. Thus, the energetics of the process should be computed directly from Eq. (7).

Assuming the Gaussian process we have

$$\hat{R}_i(\omega - \hat{\omega}, k - \hat{k}) = \frac{l_x l_t}{\pi^2}\sigma_i^2 e^{-l_t^2(\omega-\hat{\omega})^2} e^{-l_x^2(k-\hat{k})^2},$$

$$i = 0, 1, 2. \quad (13)$$

Here, l_x and l_t are the correlation length and the correlation time, respectively. The variance σ_i is approximated by σ_0 as follows:

$$\sigma_i^2 \simeq \frac{\sigma_0^2}{l_x^i}, \quad i = 1, 2.$$

The correlation length l_x, the correlation time l_t, and the variance σ_0 correspond to the size, life-time, and the flow of the granules, respectively. A typical size of the granules is about 10^3 km although smaller (larger) granules of the size 200 km ($2 \cdot 10^3$ km) are also observed. Observations show that granules have lifetimes of ~ 10 min. Larger convective motions such as mesogranules live for ~ 1 hour and supergranules of ~ 1 day lifetimes have been detected. Moreover, giant cells persisting for a solar rotation period may also exist.

As dispersion relation (7) is complex we consider first the case of a space-dependent random flow only.

3.1. Space-dependent random flow

In the case of the space dependent flow, $V_0 = V_0(x)$. This implies $\hat{\omega} = \omega$ and

$$\hat{R}_i(k - \hat{k}) = \frac{l_x}{\pi}\sigma_i^2 e^{-l_x^2(k-\hat{k})^2}, \quad i = 0, 1, 2. \quad (14)$$

We now introduce the dimensionless wave vector K and the dimensionless frequency Ω,

$$K = k l_x, \qquad \Omega = \frac{l_x}{c_0}\omega. \quad (15)$$

Using these quantities the dispersion relation (7) reads

$$\Omega^2 - K^2 = \frac{\sigma_0^2}{\pi c_0^2}[K(K - i\gamma)I_2 + (K^3 - 2iK^2 - \gamma K +$$

$$\Omega^2 K - \gamma\Omega^2)I_1 - \gamma K\Omega^2(1 + iK)I_{-1} - (K^2 + iK\Omega^2 +$$

$$\gamma^2\Omega^2 + iK^3 - K^2\Omega^2 + i\gamma K\Omega^2)I_0 + \gamma K(1 + iK)J_1 -$$

$$K(K - i)\sqrt{\pi}], \quad (16)$$

where:

$$I_n = \int_{-\infty}^{\infty} \frac{\hat{K}^n e^{-(\hat{K}-K)^2} d\hat{K}}{\Omega^2 - \hat{K}^2}, \quad n = 2, 1, 0, -1, \quad (17)$$

$$J_1 = \int_{-\infty}^{\infty} \frac{e^{-(\hat{K}-K)^2} d\hat{K}}{\hat{K}}. \quad (18)$$

These integrals can be expressed by the plasma dispersion function $Z(\xi)$ which is tabulated by Fried & Conte (1961):

$$J_1 = \sqrt{\pi} Z(-K),\ I_{-1} = \frac{2J_1 + S_1 - S_2}{2\Omega^2}, \quad (19)$$

$$I_0 = \frac{S_1 + S_2}{2\Omega},\ I_1 = \frac{S_{11} + S_{12}}{2\Omega},\ I_2 = \frac{S_{21} + S_{22}}{2\Omega}, \quad (20)$$

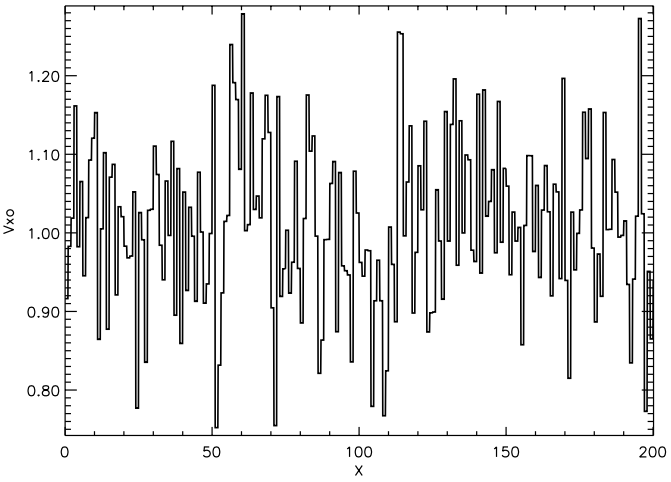

Fig. 3. Spatial derivative of a random flow, V_{0x}, for a typical realization of a medium. The spatial coordinate x is in units of the correlation length l_x and the flow V_0 is normalized by the sound speed c_0.

where:

$$S_1 = \int_{-\infty}^{\infty} \frac{e^{-(\hat{K}-K)^2} d\hat{K}}{\Omega - \hat{K}} = -\sqrt{\pi} Z(\Omega - K),$$

$$S_2 = \int_{-\infty}^{\infty} \frac{e^{-(\hat{K}-K)^2} d\hat{K}}{\Omega + \hat{K}} =$$

$$\sqrt{\pi}[2i\sqrt{\pi} e^{-(\Omega+K)^2} + Z(-\Omega^* - K)], \quad (21)$$

$$S_{11} = \int_{-\infty}^{\infty} \frac{\hat{K} e^{-(\hat{K}-K)^2} d\hat{K}}{\Omega - \hat{K}} = -\sqrt{\pi} + \Omega S_1, \quad (22)$$

$$S_{12} = \int_{-\infty}^{\infty} \frac{\hat{K} e^{-(\hat{K}-K)^2} d\hat{K}}{\Omega + \hat{K}} = \sqrt{\pi} - \Omega S_2, \quad (23)$$

$$S_{21} = \int_{-\infty}^{\infty} \frac{\hat{K}^2 e^{-(\hat{K}-K)^2} d\hat{K}}{\Omega - \hat{K}}$$

$$= -\sqrt{\pi}(K + \Omega) + \Omega^2 S_1, \quad (24)$$

$$S_{22} = \int_{-\infty}^{\infty} \frac{\hat{K}^2 e^{-(\hat{K}-K)^2} d\hat{K}}{\Omega + \hat{K}} = \sqrt{\pi}(K - \Omega) + \Omega^2 S_2. \quad (25)$$

The asterisk $*$ in Eq. (21) denotes the complex conjugate.

3.1.1. Results

While presenting all numerical results we choose a fixed sound speed $c_0 = 10\,\mathrm{km\,s^{-1}}$.

Fig. 1a shows the frequency difference $\nu - \nu_0$ as a function of the spherical harmonic degree l for $\sigma_0 = 1\,\mathrm{km\,s^{-1}}$, $l_x = 0.2$ Mm (solid line), $l_x = 1$ Mm (dotted line), and $l_x = 2$ Mm (broken line). Here, $\nu = \omega/2\pi$ is the cyclic frequency that is obtained numerically from Eq. (16) and $\nu_0 = \omega_0/2\pi = kc_0/2\pi$ pertains to the motionless equilibrium ($V_0 = 0$). The spherical harmonic degree l is related to the wave vector k through the following relation:

$$k = \frac{\sqrt{l(l+1)}}{R_s}, \quad (26)$$

where R_s is the radius of the Sun. As a result of the random velocity field the frequency ν of the random acoustic mode is lower for $l > 300$ than the frequency ν_0 of the coherent wave. For lower values of l the frequency ν is higher than ν_0. This effect is greatest for $l_x = 0.2$ Mm (solid line) for which $\nu - \nu_0$ attains its maximum at $l \simeq 50$. Such a frequency increase was already reported in the other contexts by Collin (1969), Razin (1995), Pelinovsky et al. (1998), and Murawski (2000a).

Fig. 1b presents the imaginary part of the random frequency, $Im(\nu)$, for the same values of the parameters as in Fig. 1a. As in the case of $l_x = 0.2$ Mm (solid line), $Im(\nu) > 0$ for the overall range of displayed l, the acoustic wave is unstable. The waves corresponding to $l_x = 1$ Mm (dotted line) and $l_x = 2$ Mm (broken line) are unstable for $l < 1700$ and $l < 900$, respectively. These waves are amplified by the random flow as their amplitudes grow in time. On the other hand, waves for which $Im(\nu) < 0$ are damped by the random flow as their amplitudes decrease in time. As a consequence of that we claim that granules of different size influence differently the sound waves; small granules (of the size of $l_x = 0.2$ Mm) amplify the sound waves but large granules (of $l_x = 2$ Mm) essentially damp the sound waves.

Fig. 2 displays the dependence of the acoustic wave spectrum on the variance σ_0 for the fixed value of the correlation length $l_x = 1$ Mm. As a consequence of stronger random flow the frequency ν falls more below ν_0 (Fig. 2a) in agreement with former results (e.g., Murawski 2000a,b). Acoustic waves of a negative value of $Im(\nu)$ exist for $l > 1600$ for $\sigma_0 = 0.5\,\mathrm{km\,s^{-1}}$ (solid line of Fig. 2b) and $\sigma_0 = 1\,\mathrm{km\,s^{-1}}$ (dotted line). For $l < 1600$ these waves possess a positive imaginary part of the frequency ν and consequently, they are amplified by the random flow. The wave that corresponds to $\sigma_0 = 2\,\mathrm{km\,s^{-1}}$ is amplified by the random flow for the overall values of the displayed range of l.

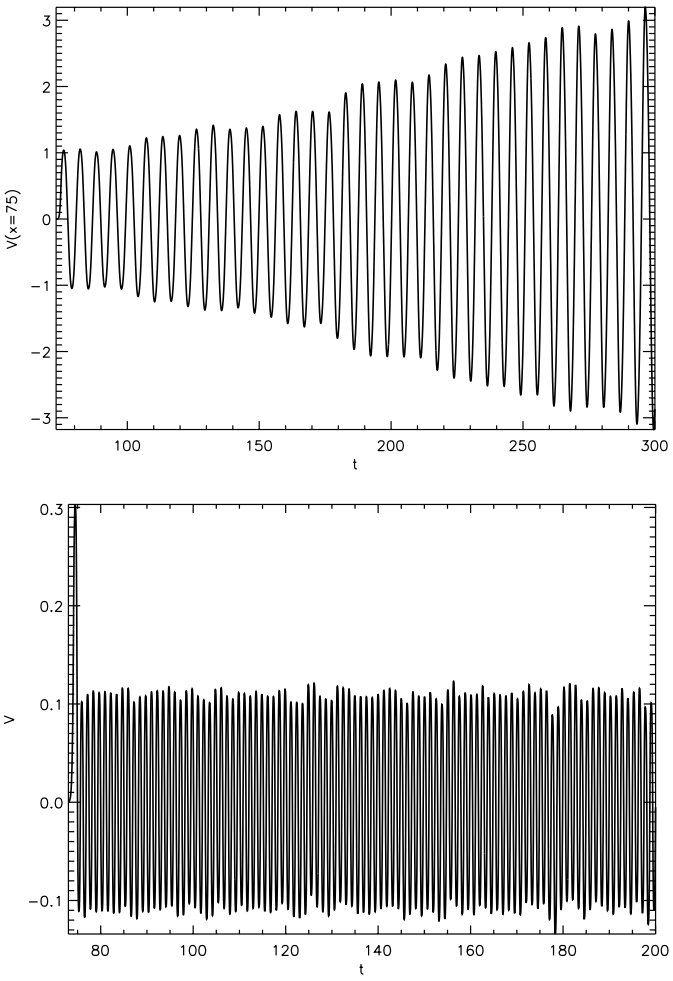

Fig. 4. Time signature of a signal which is collected at the point $x = 75$ l_x in the case of a random flow with its variance $\sigma = 0.1\ c_0$. A periodic driver, set at $x = 0$, acts with the frequency $\Omega_d = 1$ (top panel) and $\Omega_d = 5$ (bottom panel).

4. Numerical simulations

In this section we present results of numerical solutions of Eqs. (2) and (3). These simulations are performed using the CLAWPACK code (LeVeque, 1997b). This code is a collection of Fortran routines for solving a hyperbolic system of conservation laws. The general structure of the code is described in detail in the user notes written by LeVeque (1997a). The applied method is a finite volume method on a uniform rectangular grid. In this method, Eqs. (2) and (3) are discretized on a set of points: $x = j\Delta x,\ t = n\Delta t$, where j denotes the numerical cell and n corresponds to the time step. Additionally, a Riemann solver which decomposes data at cell edges into a set of waves and wave speeds is adopted. Problems with the source terms like $-V_{0x}V$ are generally solved using the Godunov splitting in which the solution of the homogeneous conservation law $V_t + AV_x = 0$ is alternated with the solution of the ordinary differential equation $V_t = -V_{0x}V$ in each time step.

In the CLAWPACK code two ghost cells are generated on each side of the computational domain which in the present approach is divided into uniform grid of $\Delta x = 0.02\ l_x$. The boundaries of the simulation box are typically placed at $x = 0$ and $x = 200\,l_x$. A periodic driver, which acts with its frequency ω_d, is set at the left boundary. In the present model the right boundaries are entirely open. So, any signal can easily cross them.

Initially, at $t = 0$, there are no signals in V and p while the flow $V_0(x)$ is set space-dependent. This flow has been chosen in such way that the V_{0x} profiles are piecewise constants (Fig. 3). As a consequence of that the flow is piecewise linear. In the regions, where $V_{0x} > 0$ ($V_{0x} < 0$), the sound waves are damped (amplified).

4.1. Numerical results and discussion

Figs. 4 and 5 present the wave profiles in the case of a periodic driver with unit amplitude and frequency $\Omega_d = 1$ (top panels) and $\Omega_d = 5$ (bottom panels) for a random flow that is shown in Fig. 3. Fig. 4 corresponds to a time-signature of the signal which is collected at $x = 75\,l_x$. As the amplitude of this signal grows in time in the case of $\Omega_d = 1$ (top panel) the sound wave

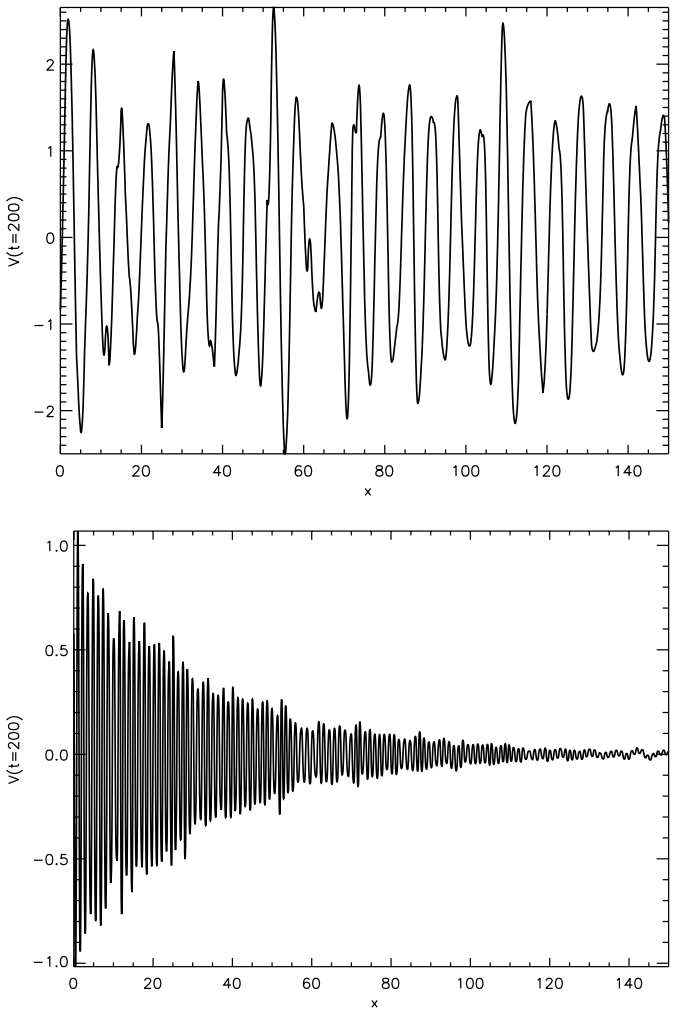

Fig. 5. Spatial wave profile at $t = 200\ l_x/c_0$ in the case of a random flow with its variance $\sigma = 0.1\ c_0$. A periodic driver, set at $x = 0$, acts with the frequency $\Omega_d = 1$ (top) and $\Omega_d = 5$ (bottom).

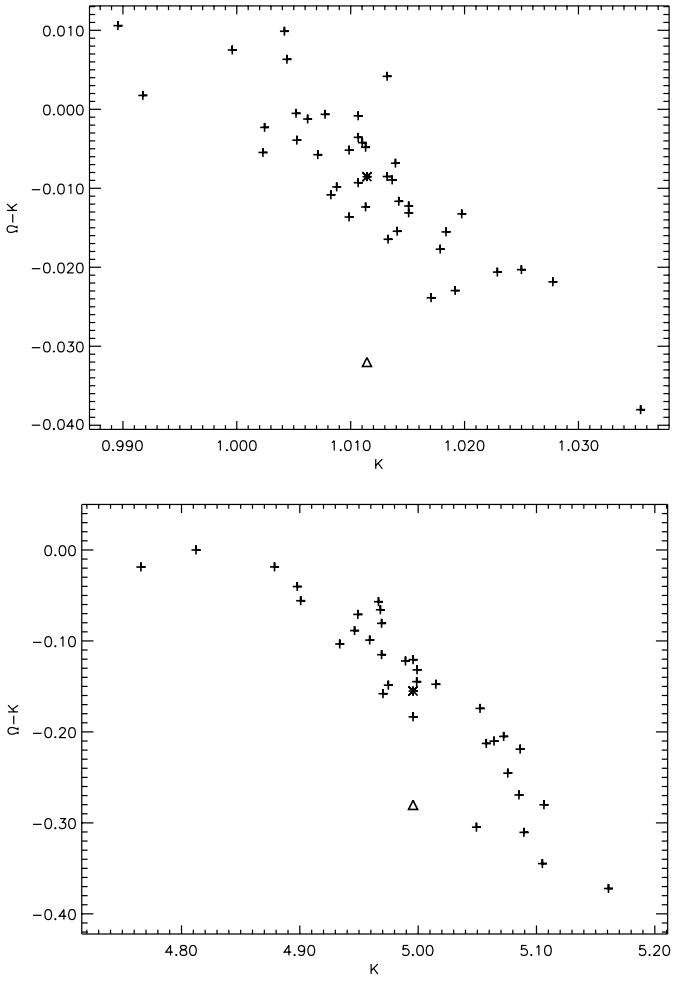

Fig. 6. Normalized frequency difference $\Omega - K$ versus dimensionless wavevector K for a random flow with its variance $\sigma = 0.1\ c_0$. The data have been obtained by numerical integration of Eqs. (2) and (3) for $\Omega_d = 1$ (top panel) and $\Omega_d = 5$ (bottom panel) and a number of realizations of the medium (the crosses). The average of the complete set of data is denoted by the asterisk. The data obtained using Eq. (16) are represented by the triangles.

is unstable. In the case of $\Omega_d = 5$ (bottom panel) the amplitude of the signal oscillates around $\sim\ 0.1\ c_0$. Fig. 5 displays the corresponding spatial profiles at the time $t = 200\ l_x/c_0$. The effect of damping is seen well in the bottom panel; the wave amplitude decreases with the coordinate x. In the case of $\Omega_d = 1$ (top panel) local amplification and damping are discernible.

The wave profiles of Figs. 4 and 5 can be analyzed spectrally to obtain the normalized frequency Ω and wavevector K, respectively. Figs. 6–8 display the results of this analysis. In particular, Fig. 6 illustrates the normalized frequency difference, $\Omega - K$ as a function of K for a number realizations of the random flow in the case of $\Omega_d = 1$ (top panel) and $\Omega_d = 5$ (bottom panel). As a result of random flows, the frequency difference for various realizations of the flow attain stochastic values; there are few realizations for which random flows speed up the sound wave but most realizations lead to a frequency decrease. There are waves of various frequencies and wavevectors being excited in different realizations. The (ensemble) averaged $\Omega - K \simeq 0.008$ is represented by the asterisk. This value is much higher than the value obtained analytically which is represented by the triangle. In the case of $\Omega_d = 5$ the ensemble averaged data (asterisk) lies closer to the analytical data (triangle) than in the case of $\Omega_d = 1$.

The difference between the analytical and numerical results is due to the approximation of a weak random flow applied in the method of Howe (1971). We expect that the results would be closer for a smaller value of σ for which the assumption of a weak random flow is more appropriate. Indeed, Fig. 7 shows that for low σ the analytical data (triangles) are closer to the numerical results (crosses) in the case of one realization of the flow.

Fig. 8 illustrates that the agreement between the numerical and analytical results depends also on the wavevector K. For low K this agreement is better. However, for $K > 5$ these two

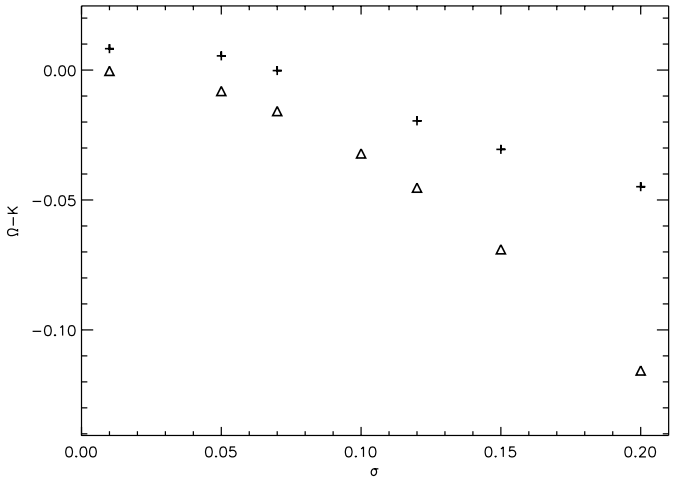

Fig. 7. Normalized frequency difference $\Omega - K$ versus dimensionless variance, σ/c_0. These data have been obtained by numerical integration of Eqs. (2) and (3) for the driving frequency $\Omega_d = 1$ and one realization of the medium (the crosses). The data obtained using the Howe method (16) are represented by the triangles.

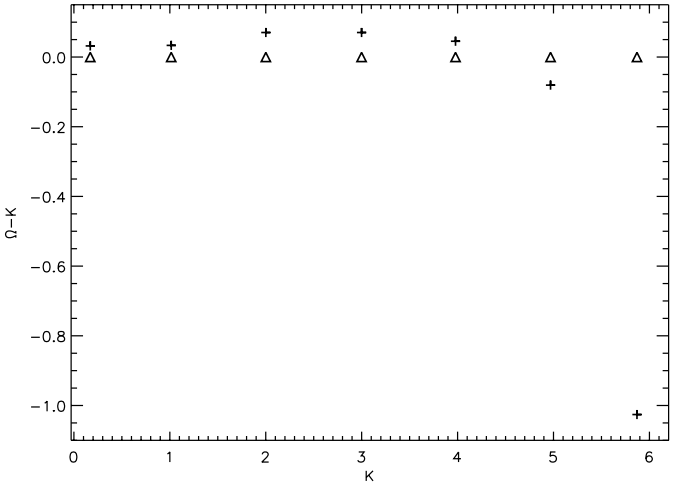

Fig. 8. Normalized frequency difference $\Omega - K$ versus dimensionless wavevector K for a random flow with its variance $\sigma = 0.1\ c_0$. These data have been obtained by numerical integration of Eqs. (2) and (3) for several values of the driving frequency Ω_d and one realization of the medium (the crosses). The data obtained using Eq. (16) are represented by the triangles.

data depart in the way that numerical data fall down abruptly in comparison to the analytical data.

5. Summary

The need for improved theoretical models of the influence of a turbulent flow on the solar acoustic waves is emphasized by recent results from helioseismology, which have provided information on the dynamics of the solar interior.

In this paper we have developed a theoretical model of the effect of random flow on the spectrum of solar acoustic oscillations. A random flow can decrease the frequencies of acoustic waves since these waves take longer to travel a given distance due to the scattering from random field (Howe 1971). However, the analytical results have also revealed that the random flow can both increase and decrease the frequencies, depending on the parameters of the flow and the spherical harmonic degree l.

The numerical simulations for a linear set of wave equations have revealed damping and amplification of the sound waves as well as frequency decrease by the random flow. The results of these simulations are in an agreement with the analytical findings for low strength of the random flow, σ.

Acknowledgements. The authors express their cordial thanks to an unknown referee for his/her constructive comment and to the Editor for his help in improving the paper. K. M.'s and J. P.'s work has been financially supported by the grant from the State Committee for Scientific Research Republic of Poland, KBN grant no. 2 PO3D 01717 and INTAS 97-31931, respectively. Numerical simulations have been performed at the Supercomputing Center of Poznań.

References

Böhmer S., Rüdiger G., 1999, A&A 351, 747
Brown T.M., 1984, Science 226/ 4675, 687
Collin R.E., 1969, Radio Sc. 4, 279
Fried B.D., Conte S.D., 1961, *The plasma dispersion function*. New York: Academic
Gough D.O., 1994, in: Zahn J.-P., Zinn-Justin J. (eds.), Astrophysical Fluid Dynamics. Amsterdam: Elsevier
Gruzinov A.V., 1998, ApJ 498, 458
Howe M.S., 1971, J. Fluid Mech. 45, 785
Joarder P.S., Nakariakov V.M., Roberts B., 1997, Solar Phys. 176, 285
Kosovichev A.G., 1995, Proc. 4th SOHO Workshop, ESA SP-376, Noordwijk: ESTEC
Lavely E.M., Ritzwoller M.H., 1992, Phil. Trans. R. Soc. Lond. A339, 413
Leighton R.B., Noyes R.W., Simon G.W., 1962, ApJ 135, 474
LeVeque R.J., 1997a, CLAWPACK User Notes, Applied Mathematics. Seattle: Univ. of Washington
LeVeque R.J., 1997b, J. Comp. Phys. 131, 327
Murawski K., 2000a, A&A, in press
Murawski K., 2000b, ApJ, in press
Nakariakov V.M., Roberts B., 1995, Solar Phys. 159, 213
Nakariakov V.M., Roberts B., Murawski K., 1998, A&A 332, 795
Pelinovsky E.N., 1979, Wave propagation in statistically inhomogeneous ocean, in: Nonlinear Waves. Moscow: Nauka
Pelinovsky E., Razin A.V., Sasarova E.V., 1998, Waves in Random Media 8, 255
Rabinovich M.I., Trubetskov D.I., 1989, Oscillations and Waves in Linear and Nonlinear Systems. Dordrecht: Kluwer Acad. Publ.
Razin A.V., 1995, Waves in Random Media 5, 137
Swisdak M., Zweibel E., 1999, ApJ 512, 442
Ulrich R.K., 1970, ApJ 162, 993
Zhugzhda Y.D., 1998, A&A 332, 314